MONITORING THE DYNAMICS OF THE SURFACE DEFORMATION PRIOR TO THE ONSET OF PLASMA EMISSION DURING FEMTOSECOND LASER ABLATION OF NOBLE METALS BY TIME-RESOLVED REFLECTIVITY MICROSCOPY

I. Carrasco-García, José M. Vadillo, J. Javier Laserna

Universidad de Málaga, UMALASERLAB, Jimenez Fraud 4, ES 29010

ABSTRACT

The generation of an expanding plasma during laser ablation is preceded at early times by the formation and evolution of a subsurface melted front. The monitoring of such transient event can´t be studied by conventional spectroscopic techniques. Pump-probe femtosecond microscopy allows the following of the surface changes during femtosecond laser ablation taking advantage of the formation of a number of dynamic Newton rings that evolve with time. Measurements at different times allow the quantification of the radial expansion velocity of the molten material. For Au and Ag, expansions in the range of 7000-12000 m/s for Au and 3000-21000 m/s have been calculated depending on the pump energies. Such values corresponds to hypersonic velocities with Mach number between 3 and 6.

KEYWORDS

Femtosecond laser ablation; Pump-probe spectroscopy; Newton rings; Laser-matter interaction.

INTRODUCTION

Laser-induced phase changes occur during laser-matter interaction as long as a certain fluence (energy density) threshold is reached. Depending on the energy involved during the interaction, the system may irreversibly evolve to complete phase-explosion and the formation of an expanding plasma.

Femtosecond laser ablation induces excitation in the target at a timescale shorter than thermal processes. Figure 1 sketches the temporal frame of the early events occurring at the sample microscopic level before the starting of the plasma formation.[1] A variety of thermal and structural effects are temporally gaped from the initial photon absorption by the target (double arrow line in figure 1) in a timescale of tens of picoseconds. Under such early non-thermal processes, the lattice of the target remains intact during the pulse.[2] Thus, as long as a sub-picosecond time resolution is attainable, an unsurpassable opportunity of an individual study of the temporal evolution of the sample surface after laser irradiation covering from early photons absorption to the onset of a laser-produced plasma is feasible. Obviously, ultrafast recording system is needed to register the transient process. Time-resolved reflectivity measurements coupled to ultrafast photodiodes or streak cameras[3] have allowed the determination of variations in the native reflectivity of materials after laser irradiation in order to relate them with the induced processes. Shadowgraphies of the sample surface at grazing angle using a picosecond-resolved pump-probe scheme[4] permitted a sound study of the dynamic of the plasma and the establishment of the importance of early electrons released from the sample surface at sub-nanosecond time-scale. Earlier, time-resolved electron diffraction was used to determine laser-induced phase changes.[5] However, time-resolved microscopy of the changes induced in the sample surface just can be obtained by combining a femtosecond pump-probe excitation/illumination scheme with a zenital-view microscopy observation. Since its development the technique has turned a significant tool to reveal the dynamics of laser-matter interaction. Particularly interesting is the evidence of the formation of a characteristic ring pattern (dynamic Newton´s rings) with a defined changing pattern as the laser-matter interaction process evolves.[6] The

origin of the dynamic rings is based on the existence in the irradiated area of an optical multilayer system (air, laser-altered sample and unaltered sample) that act as a thin-film interferometer.[7] A sequence of dark and bright rings can be observed within the irradiated region, whose number, width, and optical contrast depend on the material, pulse duration, and laser fluence. The observed pattern changes significantly as a function of sample type or applied fluence[8,9] and so, under a set of excitation conditions, the modification in the Newton´s rings can be unequivocally related to the material being inspected.

Newton rings change dynamically as the subsurface molten layer does, and in this sense, represent an interesting tool to study phenomena related to laser-matter interaction that can´t be revealed by conventional approaches. Among other, Newton rings allows for the calculation of the subsurface expansion of the melted front and the parameters affecting its dynamics. Such measurements are of importance as the expansion parameters of the melted front can be related to the final volume of the ablation craters and provide useful information about the intermixing zone and the alloying processes. Also, the dynamic of the rings may be significantly affected by the depth of the ablated layer, particularly in very thin films and more interestingly, in multilayered thin-films.

Noble metals exhibit excellent electron mobility and are used in many applications in strategic fields as photonics or nanoplasmonics as thin layers. The dynamic measurements by phase-change microscopy should be significantly affected by drifts from the pristine original material. Our study may allow the establishing of connections between compositional or structural changes in the sample with the dynamic of the rings. Two noble metals thin films (Au and Ag) have been studied at a range of fluences above plasma threshold during the first nanosecond of the laser-matter interaction. Such time span allows the recording from the early electron excitation to the onset of plasma formation.

EXPERIMENTAL

The experimental set-up is has been detailed in a previous reference.[9] Briefly, it consists on a Ti:Sa femtosecond laser (MaiTai, Spectra-Physics) centered at 800 nm with a bandwidth of 60 nm, that is delivered into a regenerative amplifier (Spitfire XP, Spectra Physics) to generate p-polarized 3,5 mJ pulses of 35 fs at a repetition rate between 4 Hz and 1 KHz. The beam is split into two branches (pump and probe) of different energy. The length of optical path in both branches can be varied independently by means of mirrors in retro reflecting configuration up to a maximum distance of 50 cms, allowing time-differences up to 3 ns between them. The beam was delivered to the sample through different mirrors and attenuation elements before being focused through a f=200mm plane-convex lens into the sample at an incidence angle of 45º. A mechanical shutter allows the selection of individual pulses for the pump branch.

The probe beam was doubled in frequency making use of a harmonic generator to generate a beam centered at 400 nm. The probe beam was then directed through the back face of a dichroic mirror into a 20x Plan APO microscope objective onto the target at normal incidence. The light collected from the objective was reflected by a dichroic mirror to reject wavelengths different than 400 nm and was 1:1 imaged through a plane-convex lens to the focal plane of a 10-bits CMOS camera. The CMOS camera was synchronized with the electromechanical shutter to allow the different time windows to monitor the temporal evolution of laser ablation.

Data processing of the micrographs was performed with a home-written script capable of selecting an area of interest and the calculation of the normalized reflectivity over an average of 400 pixels on the center of each micrograph. The whole process implies the acquisition of three consecutive images in the following workflow: firstly, the target was captured before irradiation and used as background, followed by a second micrograph showing the changes taking place at a specific delay, and a final micrograph showing the permanent morphological alterations several seconds after the exposure to the laser irradiation.

The target was set on a XYZ stage for selecting a new clean area at every shot. The assurance of a flat surface is critical as the light-surface transient effect observed can be significantly affected. Figure 2 show the dramatic differences occurring in the same substrate (a photovoltaic-grade silicon wafer) subjected to two different processes: a chemical texturing process that generates a surface roughness of about 5 microns, and a mechanical mirror-polishing to decrease the roughness down to 10 nm. As observed, the reflectivity of the textured sample is quite low, showing neither any remarkable feature nor a time-dependence. On the contrary, in the highly polished sample the differential light reflectance is visible, exhibiting a remarkably different spatial and temporal behavior that evidences different excitation mechanisms, as will be commented later. Given such evidences, care was taken to minimize roughness in the 200-nm thick Au and Ag samples used. The preparation was made by DC sputtering on microscope cover slides with nominal roughness lower than 5 nm. The reflectivity measurements and time-dependence behavior of our Au and Ag thin-layers are assumed to be quite transferable to those on thick pure metal foils based on previous references.[10] A coarse plasma formation threshold was established at an energy of 150 μJ (1.5 J/cm^2) based on the appearance of a tiny spark at the sample surface. A previous manuscript[11] with the same laser source based on spectroscopic detection following a signal-to-noise criteria, reported a energy of 50 μJ (4 J/cm^2) for the plasma ignition threshold using normal incidence. The differences in the fluence value must be attributed to the different irradiated area, a phenomena previously reported[12] under nanosecond excitation.

RESULTS AND DISCUSSION

The timing calibration of the experiment was performed with polished Si following the procedure described in our previous publication[9]. After proper adjustment of the delay lines, Au and Ag samples were studied. Based on previous references[4], processes previous to plasma formation occur during the first 100 ps of laser-matter interaction lifetime. Comparison of the micrographs in Figure 3 allows the observation of a rapid increase of the reflectivity in both materials that remains at least during the first two picoseconds after irradiation. Such increase, in experimental coincidence with other authors,[3,6] is due to the electron-hole plasma generated as a consequence of the high intensities applied during femtosecond irradiation and the low electron heat capacity of the solid.[13] Meanwhile, the lattice can be considered unaffected just after the end of the laser pulse, and the heating of the lattice can be studied as a separated effect from the electron plasma as described in the two temperature model.[14,15] After the increase of the electronic density on the surface, electrons de-excite and start heating the lattice by electron-phonon collisions, leading the different mechanisms related to the onset of plasma formation as long as the fluence is high enough. By experimental spectroscopic methods, the presence of detectable photons, ions or electrons are used to determine the energy threshold.[12,16] However, the timing of the process is much more difficult to establish. In our approach, the starting of the plasma formation may be assigned to a decrease of the reflectivity in the central area of the target due to a strong absorption of the incident probe light that expands outwards.

A quantitative description of the excitation and the onset of ablation can be provided from measurements of the normalized reflectivity of the targets at different fluences as a function of time. Figure 4 shows the differences between both metals when exposed to identical pump and probe conditions. In order to assure sub- and over-threshold excitation conditions, 50 μJ (0.5 J/cm^2) and 200 μJ (2.0 J/cm^2) were used. In both cases the probe beam was set at 10 μJ and fired with an interpulse delay of 1 ns. It is quite evident that Au films develop a higher number of rings than Ag

and are better contrasted. Detailed post-processing of the information included in the micrographs allows to follow the time evolution of sample reflectivity.

The normalized reflectivity has been recorded by averaging 400 pixels in the center of each micrograph, following described procedures.[9,17,18] As free electrons of metals absorb the laser radiation while the lattice remains cold, the energy is distributed by collisions among the electrons, and induce a thermalization of the electron gas on a femtosecond timescale,[19] which is in agreement with the increase of the reflectivity seen in our results for both metals up to the first picosecond. Due to the similar properties of Au and Ag, significant differences were not expected in their respective behaviors. Figure 5 shows the evolution of the relative surface reflectivity with interpulse time in Au and Ag. As observed, the increase of reflectivity occurs at the same delay time regardless the fluence of the pump beam, and the shape of the curves are identical. Concerning the falling edge of the curve, again the behavior is identical between metals in the whole fluence range studied. As observed, both metals experience a drop in the reflectivity after the maximum, switching to negative values at about 5 ps. This negative data on the reflectivity are related to the description mentioned in Figure 3 for the onset of ablation. The reflectivity measurements remain in negative values as a plateau up to the nanosecond time-scale.

The recording of micrographs at longer delays allows the observation of the dynamic Newton rings. In a previous study on silicon it has been reported that the onset of the rings is related to the fluence,[9] and once the plasma formation threshold is exceeded, the observation of the rings takes place on the periphery instead of the whole irradiated area. In Figure 5 it has been indicated the time at which the first Newton ring in is observed both metals. As shown, the first ring appears at a delay of about 350 ps in Au, whereas it requires 700 ps to be visible in Ag.. Both metals at 800 nm show almost identical refractive index (n_{Ag}: 0.186, n_{Au}: 0.188) and extinction coefficients (k_{Ag}: 4.98, k_{Au}: 4.70)[20] and so, any optical effect associated to the pump beam should be initially ruled out. At the wavelength of the probe beam (400 nm), the extinction coefficients are quite similar too (k_{Ag}: 1.90, n_{Au}: 1.83), but there is a significant difference in the refractive index (n_{Ag}: 0.14, n_{Au}: 1.53)[20]. However,

the probe energy is way lower than that required to induce any significant excitation out of the sample. On the other hand, it is not clear how a change in the refraction index could explain an earlier expansion of the molten interface. The explanation could rely on the different electronic properties of both systems as the early stages of femtosecond laser ablation are governed by electron heating.

Post processing of the time-resolved micrographs allows collecting useful information on the dynamics of the expansion process occurring in the subsurface molten layer. Figure 6 shows a sequence of pictures taken at different delay times (from 20 ps to 1.2 ns) on Au after excitation with the pump beam at 150 μJ. The reflectivity intensity profile along the major axis was extracted and it is represented for each micrograph. For a more intuitive comparison, the origin of the x-axis has been assigned to the geometrical center of each image. It is very clear the expansion of the affected area as time increases. As observed, in the interval from 20 ps to 250 ps, the affected area has doubled its size, evidencing the dynamic process occurring during the early laser interaction with the sample. Such expansion is also evident in the dynamics of the Newton rings. As observed in the figure, the Newton rings (identified with numbers) increase their diameter with time. Up to three Newton rings have been completely monitored. As the x-axis scale is identical for all the figures, the displacements in the centroids can be related unequivocally with actual expansion speed of the Newton rings from the center to the periphery. Considering the interferometric origin of the Newton rings, the determination of the expansion speed is directly related to the 3D expansion of the molten layer. The flat central region of the intensity profiles exhibits negative reflectivity, in accordance with the formation of a high density electron plasma on the surface of the molten layer that absorbs the probe beam.[21] The reduced laser energy in the tails of the incoming Gaussian beam allows the observation of the ring pattern in the periphery of the images.

The variation of the first Newton ring as a function of delay time for Au at different fluence values is shown in Figure 7. As observed, the trend is linear, evidencing the expansion process taking place. Each point corresponds to the average of three independent data sets. The slope of the fitting line represents the average expansion speed of the molten layer at the different fluence values.

Expansions in the range of 7000-12000 m/s for Au and 3000-21000 m/s for Ag have been calculated. Considering the dependence of waves propagation with solids, the expansion speed data were corrected with the respective sound speed for Au (2030 m/s) and Ag (2680 m/s) to obtain the Mach number in each case. The data are shown in Figure 8, where Mach number as high as 6 can be obtained. High Mach numbers can be found in the literature,[22] evidencing the formation of high-pressure shockwaves of several GPa. In broad terms, it can be concluded that the 1st rings expands with an average Mach number of 2, while the 2nd rings does it with an average Mach number around 4. It is important to consider that the radial expansion measured from a 2D projection on the CCD sensor corresponds to a 3D object that exhibits a z-axis displacement with time. In this sense, the higher expansion speed in the second ring, could be simply due to an additional contribution of the shrinkage of the melted zone in the Z-axis direction. In any case, the evidence of hypersonic expansion of the melted zone is clear. Further work is in progress to understand the dependence of these values with sample type, and the possible effect of compositional changes and dynamics of the surface deformation prior to the onset of plasma emission.

CONCLUSIONS

Generation of an expanding plasma following laser ablation is preceded at early times by the formation and evolution of a subsurface molten phase. Monitoring of such transient events are difficult to study by conventional spectroscopic techniques. Pump-probe femtosecond microscopy constitutes an important tool for observing and understanding how the surface evolves after ultrafast excitation. Measurements at different times allow the quantification of the radial expansion velocity of the molten material which finally leads to phase explosion and plasma emission. For Au and Ag, expansions in the range of 7000-12000 m/s for Au and 3000-21000 m/s have been calculated depending on the pump energy. Such values correspond to hypersonic velocities with Mach number between 3 and 6.

ACKNOWLEDGEMENTS

This work has been funded by the Spanish Ministry of Economy and Competitiveness (MINECO) through projects CTQ2011-24433 and CTQ2014-56058P. One of the authors (ICG) acknowledges the financial support of her doctoral work through the Programa de Formación de Personal Investigador.

REFERENCES

1. S.K. Sundaram, E. Mazur, Inducing and probing non-thermal transitions in semiconductors using femtosecond laser pulses, Nat. Mater. 1 (2002) 217-224, http://dx.doi.org/10.1038/nmat767.

2. E.G. Gamaly, A.V. Rode, Physics of ultra-short laser interaction with matter: From phonon excitation to ultimate transformations, Progress in Quantum Electronics 37 (2013) 215-323, http://dx.doi.org/10.1016/j.pquantelec.2013.05.001.

3. J. Bonse, G. Bachelier, J. Siegel, J. Solis, Time- and space-resolved dynamics of melting, ablation, and solidification phenomena induced by femtosecond laser pulses in germanium, Phys. Rev. B 74 (2006) 134106, http://dx.doi.org/10.1103/PhysRevB.74.134106.

4. S. S. Mao, X. Mao, R. Greif, R. E. Russo, Initiation of an early-stage plasma during picosecond laser ablation of solids, Appl. Phys. Lett. 77 (2000) 2464-2466, http://dx.doi.org/10.1063/1.1318239.

5. S. Williamson, G. Mourou, J.C.M. Li, Time-Resolved Laser-Induced Phase Transformation in Aluminum, Phys. Rev. Lett. 52 (1984) 2364—2367, http://dx.doi.org/10.1103/PhysRevLett.52.2364.

6. K. Sokolowski-Tinten, J. Bialkowski, A. Cavalleri, M. Boing, H. Schüler, D. von der Linde, Dynamics of femtosecond-laser-induced ablation from solid surfaces, Proc. SPIE 3343 (1998), High-Power Laser Ablation 46. http://dx.doi.org/10.1117/12.321593.

7. J. Hernandez-Rueda, J. Siegel, M. Garcia-Lechuga, J. Solis, Femtosecond laser-induced refractive index changes at the surface of dielectrics: quantification based on Newton ring analysis, J. Opt. Soc. Am. B. 31 (2014) 1676-1683. http://dx.doi.org/10.1364/JOSAB.31.001676.

8. M. Schmidt, M. Zaeh, T. Graf, A. Ostendorf, Matthias Domke, Gerhard Heise, Isabel Richter, Sebastian Sarrach, Heinz P. Huber, Pump-Probe Investigations on the Laser Ablation of CIS Thin Film Solar Cells, Physics Procedia 12 (2011) 396-403, http://dx.doi.org/10.1016/j.phpro.2011.03.149.

9. I. Carrasco-García, J. M. Vadillo, J. J. Laserna, Visualization of surface transformations during laser ablation of solids by femtosecond pump–probe time-resolved microscopy, Spectrochimica Acta Part B 113 (2015) 30–36, http://dx.doi.org/10.1016/j.sab.2015.08.009.

10. J. Hohlfeld, J.G. Müller, S.S. Wellershoff, E. Matthias, Time-resolved thermoreflectivity of thin gold films and its dependence on film thickness, Applied Physics B 64 (1997) 387-390, http://dx.doi.org/10.1007/s003400050189.

11. Marina López-Claros, José M. Vadillo and J. Javier Laserna, Determination of plasma ignition threshold fluence during femtosecond single-shot laser ablation on metallic samples detected by optical emission spectroscopy, J. Anal. At. Spectrom. 30 (2015) 1730, http://dx.doi.org/10.1039/c5ja00076a.

12. José F. Alcántara, José M. Vadillo and J. Javier Laserna, Experimental variables and matrix effects associated with the onset of ion generation in laser ionization of solid samples, J. Anal. At. Spectrom. 25 (2010) 1424-1431, http://dx.doi.org/10.1039/B921969B.

13. E. G. Gamaly, A. V. Rode, B. Luther-Davies, V. T. Tikhonchuk, Ablation of solids by femtosecond lasers: Ablation mechanism and ablation thresholds for metals and dielectrics, Phys. Plasmas 9 (2002) 949-957, http://dx.doi.org/10.1063/1.1447555.

14. B. N. Chichkov, C. Momma, S. Nolte, F. von Alvensleben, A. Tünnermann, Femtosecond, picosecond and nanosecond laser ablation of solids, Appl. Phys. A 63 (1996) 109-115, http://dx.doi.org/10.1007/BF01567637.

15. S. Nolte, C. Momma, H. Jacobs, A. Tünnermann, B. N. Chichkov, B. Wellegehausen, H. Welling, Ablation of metals by ultrashort laser pulses, J. Opt. Soc. Am. B 14 (1997) 2716-2722, http://dx.doi.org/10.1364/JOSAB.14.002716.

16. José M. Vadillo, Carmen C. García, José F. Alcántara, J. Javier Laserna, Thermal-to-plasma transitions and energy thresholds in laser ablated metals monitored by atomic emission/mass spectrometry coincidence analysis, Spectrochimica Acta. Part B 60 (2005) 948-954, http://dx.doi.org/10.1016/j.sab.2005.06.003.

17. J. Siegel, D. Puerto, W. Gawelda, G. Bachelier, J. Solis, Plasma formation and structural modification below the visible ablation threshold in fused silica upon femtosecond laser irradiation, Appl. Phys. Lett. 91 (2007) 082902, http://dx.doi.org/10.1063/1.2766848.

18. D. Puerto, J. Siegel, W. Gawelda, M. Galvan-Sosa, L. Ehrentraut, J. Bonse, J. Solis, Dynamics of plasma formation, relaxation, and topography modification induced by femtosecond laser pulses in crystalline and amorphous dielectrics, J. Opt. Soc. Am. B 27 (2010) 1065-1076, http://dx.doi.org/10.1364/JOSAB.27.001065.

19. B. Rethfeld, A. Kaiser, M. Vicanek, G. Simon, Ultrafast dynamics of nonequilibrium electrons in metals under femtosecond laser irradiation, Phys. Rev. B 65 (2002) 214303, http://dx.doi.org/10.1103/PhysRevB.65.214303.

20. Handbook of Optical Constants of Solids, edited by E.D. Palik, Academic Press, Boston, 1985, ISBN 9780080547213, http://dx.doi.org/10.1016/B978-0-08-054721-3.50001-0.

21. Tae Y. Choi, Costas P. Grigoropoulos, Plasma and ablation dynamics in ultrafast laser processing of crystalline silicon, Journal of Applied Physics 92 (2002) 4918, http://dx.doi.org/10.1063/1.1510565.

22. T. Pezeril, G. Saini, D. Veysset, S. Kooi, P. Fidkowski, R. Radovitzky, and Keith A. Nelson, Direct Visualization of Laser-Driven Focusing ShockWaves, Phys. Rev. Lett. 106 (2011) 214503, http://dx.doi.org/10.1103/PhysRevLett.106.214503.

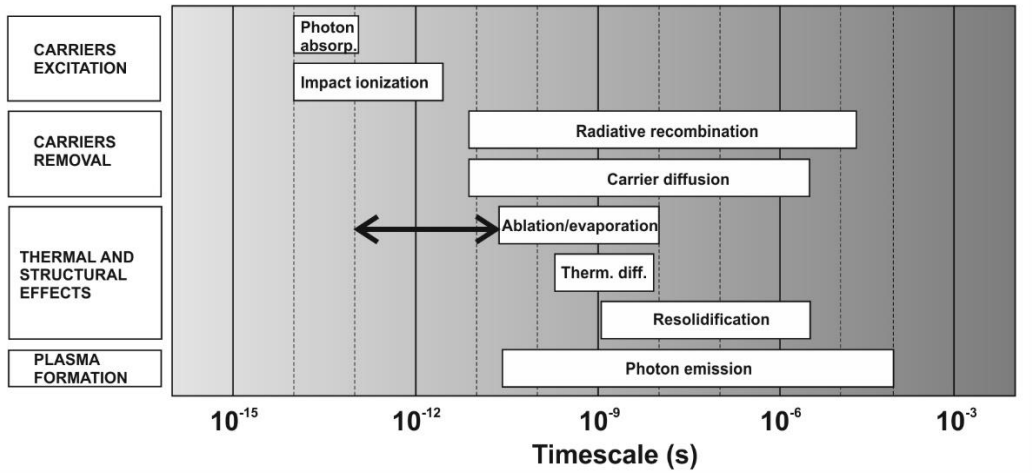

Figure 1. Sketch of early processes during laser-matter interaction. Adapted from Sundaram and Mazur.[1]

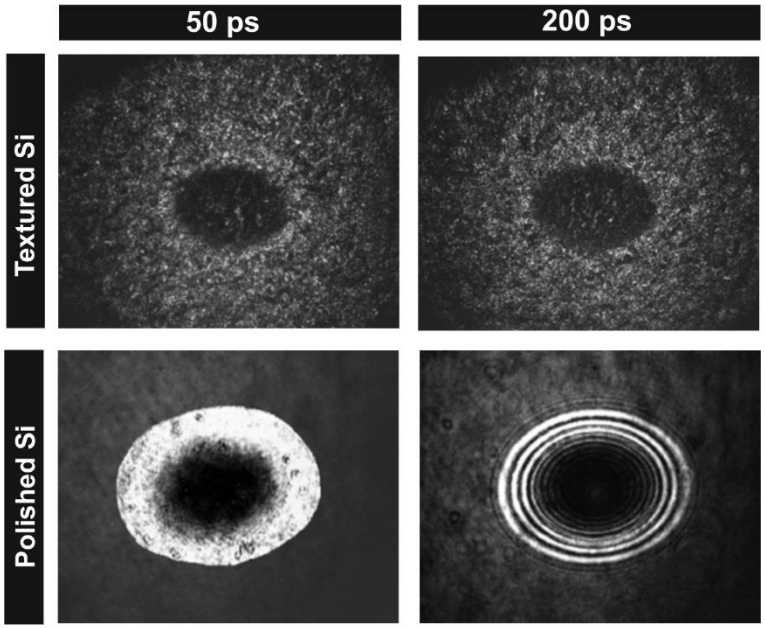

Figure 2. Effect of native roughness on time-resolved surface reflectivity at 400 nm. See sample details in the text.

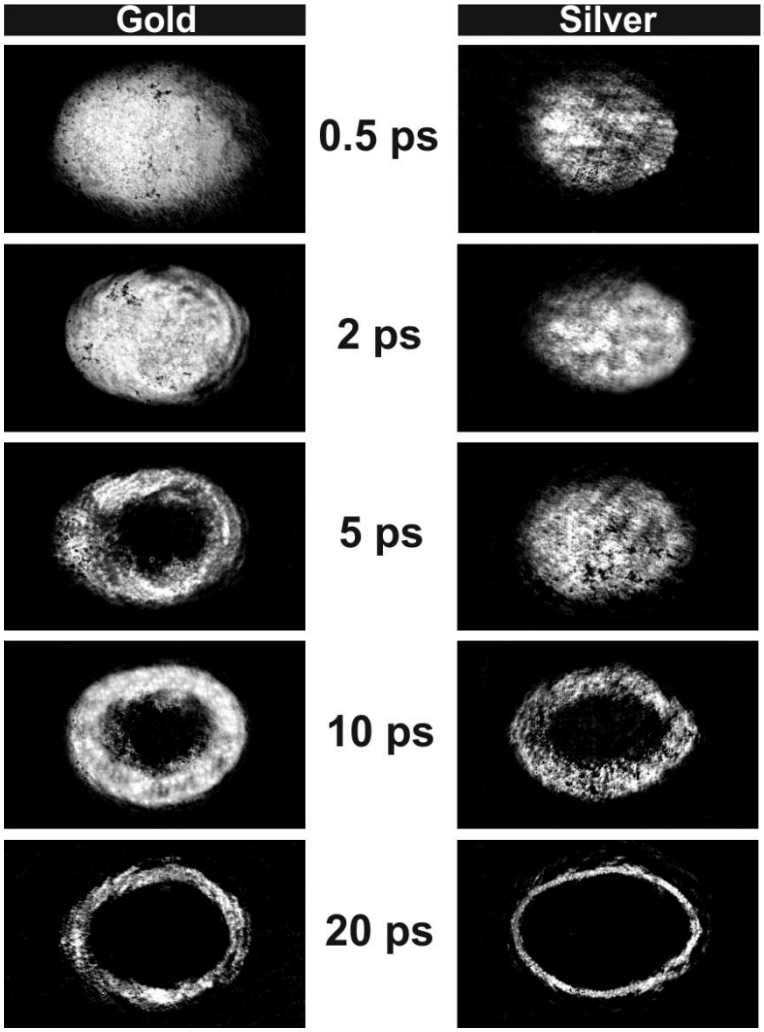

Figure 3. Comparison of relative surface reflectivity images (ΔR/R) for gold (left column) and silver (right column) at a λ_{probe}= 400 nm at different delay times after exposure to the pump pulse (λ_{pump}= 800 nm, 150 μJ/pulse, 1.5 J/cm^2). The intensity is encoded in a linear gray scale. See additional information in the text.

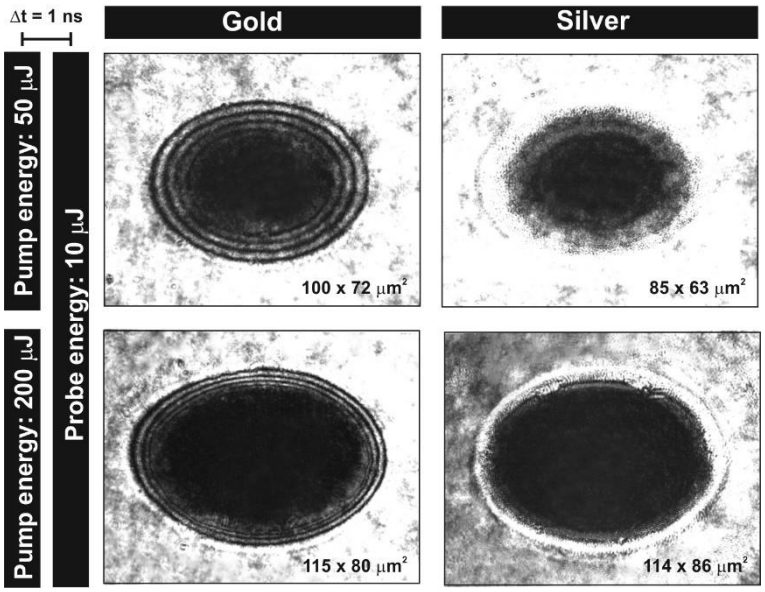

Figure 4. Comparison of relative surface reflectivity images (ΔR/R) for gold (left column) and silver (right column) at a λ_{probe}= 400 nm at two different pump energies: 50 μJ (0.5 J/cm^2) and 200 μj (2.0 J/cm^2). The images were taken at a delay time of 1 ns after exposure to the pump pulse (λ_{pump}= 800 nm, 150 μJ/pulse, 1.5 J/cm^2). The intensity is encoded in a linear gray scale. See additional information in the text.

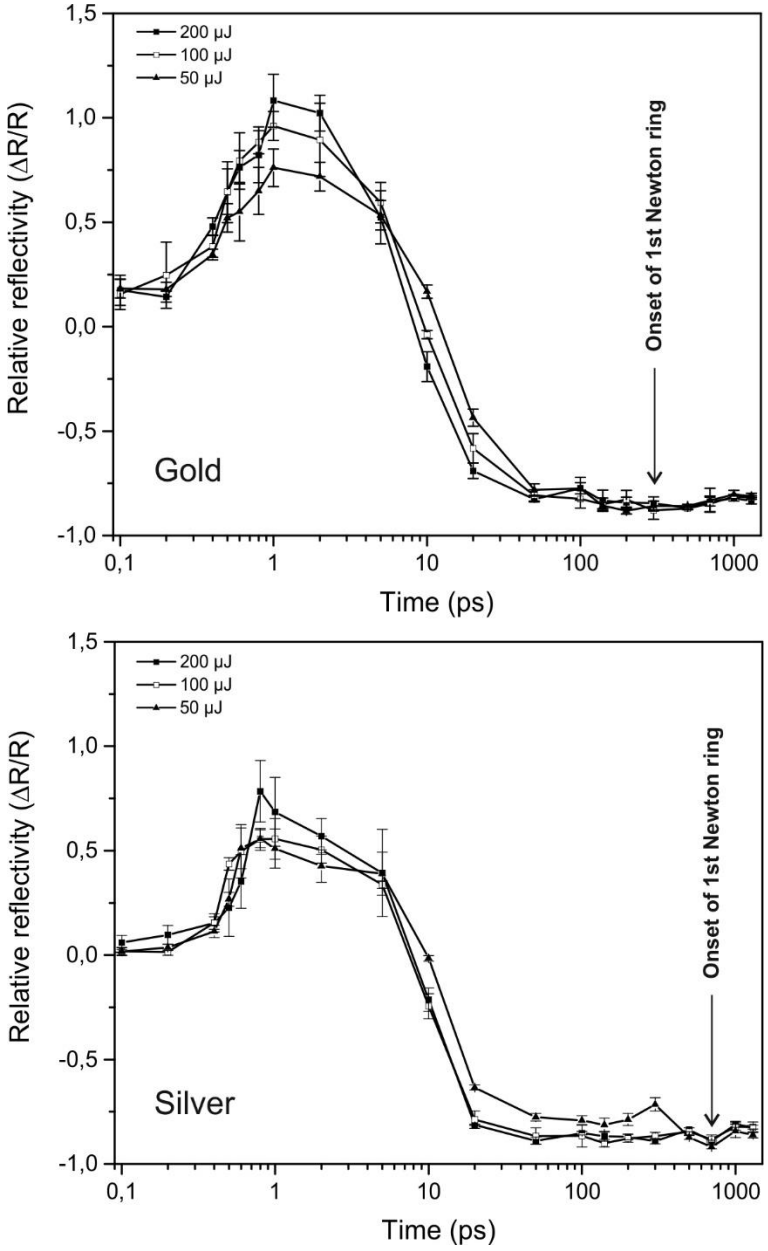

Figure 5. Evolution of relative surface reflectivity (ΔR/R) in gold (top) and silver (bottom) during the first 1200 ps after arrival of the pump pulse. Each point represents the averaging of three measurements on fresh sample locations (standard deviation is indicated as vertical bars). Data sets represent the measurements at three pump fluence conditions. See additional explanations in the text.

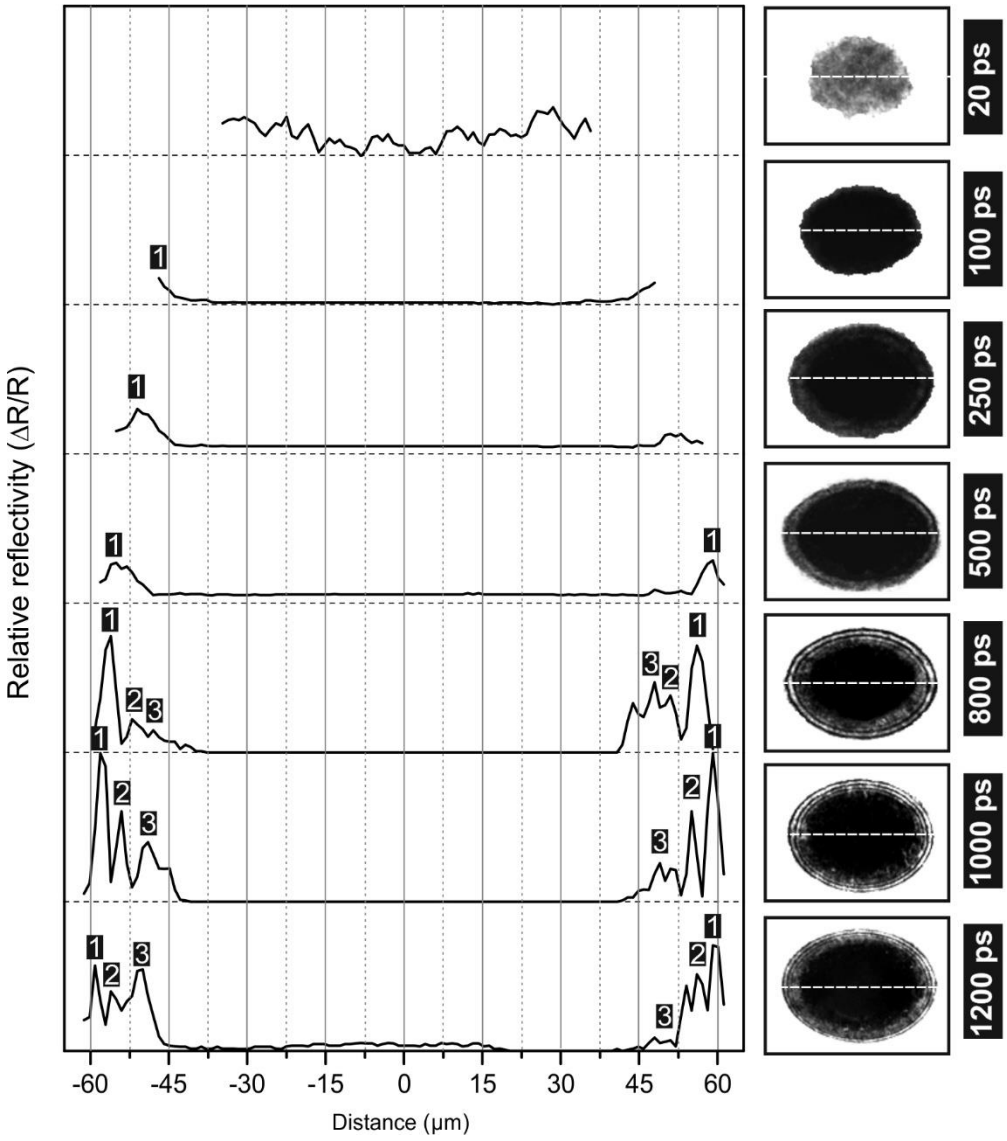

Figure 6. Scan profiles of the relative surface reflectivity (ΔR/R) in gold along the horizontal axis (dotted line) in the time-resolved micrographs at a pump energy of 150 μJ (1.5 J/cm^2). The Y-axes in the plots have been normalized to 256 grey levels. The position of the 1st, 2nd and 3rd Newton rings are indicated with numbers. See additional information in the text.

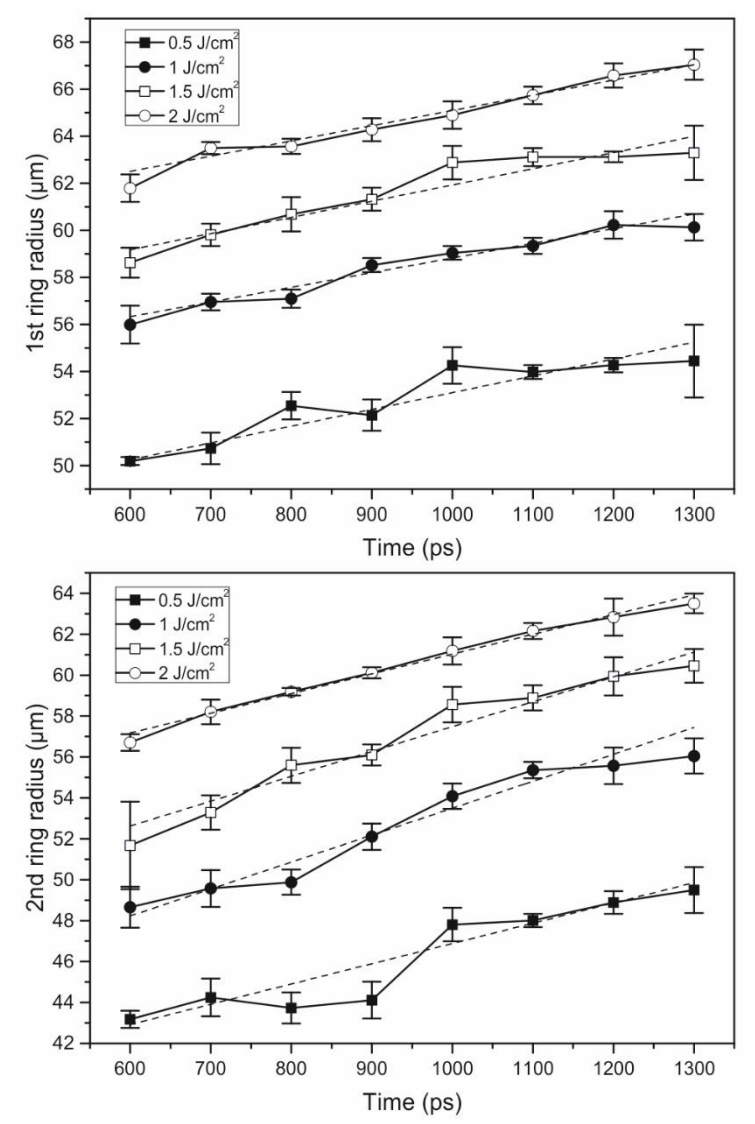

Figure 7. Lateral displacement of the 1st Newton ring in gold as a function of time under four different fluence conditions of the pump pulse. Each data point corresponds to the averaging of three independent measurements of fresh surfaces. Standard deviation is indicated as vertical bars. The slope of the fitting line for each data set was taken as the average expansion speed. See text for additional details.

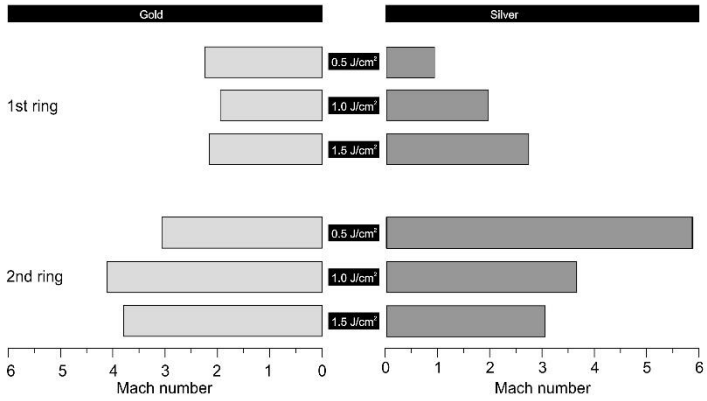

Figure 8. Comparative of the expansion speed of the 1st and 2nd Newton rings in gold and silver at three different pump laser fluences. Considering the different sound speed in Au and Ag, data are shown in normalized Mach numbers.